A CHA zeolite supported Ga-oxo cluster for partial oxidation of CH_4 at room temperature

Shunsaku Yasumura[a], Mengwen Huang[a], Xiaopeng Wu[a], Chong Liu[a], Takashi Toyao[a,b], Zen Maeno[a]*, Ken-ichi Shimizu[a,b]*

[a] Institute for Catalysis, Hokkaido University, N-21, W-10, Sapporo 001-0021, Japan

[b] Elements Strategy Initiative for Catalysts and Batteries, Kyoto University, Katsura, Kyoto 615-8520, Japan

*Corresponding authors

Zen Maeno E-mail: maeno@cat.hokudai.ac.jp

Ken-ichi Shimizu E-mail: kshimizu@cat.hokudai.ac.jp

Keywords:

CH_4 activation, Ga-exchanged zeolite, Multinuclear Ga-oxo cluster, *in situ* XAFS, DFT calculation

Abstract

A catalytic system for activation of CH_4 under mild conditions is in high demand. In this study, Ga-oxo clusters in CHA zeolites were prepared by reductive solid-state ion-exchange followed by O_2 treatment. Formation of the Ga-oxo clusters was demonstrated using X-ray absorption fine structure (XAFS) measurements. Plausible models of the cluster were developed by using an *ab initio* thermodynamic analysis. Importantly, the CHA zeolite-supported Ga-oxo clusters promote partial oxidation of CH_4 to yield adsorbed formaldehyde and formic acid. The results of density functional theory (DFT) calculations, designed to gain information about the mechanism of the process, show that the $[Ga_2(O)(OH)_2]^{2+}$ ion is likely the most active cluster for C–H bond activation of CH_4. Observations made in this experimental and theoretical effort demonstrate that main-group metal-oxo clusters have the potential of serving as active species for transformations of CH_4.

1. Introduction

CH_4 is an abundant natural resource present in shale gas. Although, various homogeneous and heterogeneous catalysts have been developed to activate the C–H bond in CH_4 for functionalization, most require high temperatures [1]. Thus, new methods for CH_4 activation under mild conditions are in great demand. Zeolite-supported metal catalysts have attracted significant attention in this context [2-14]. For example, O_2-activated Cu-zeolites are well-known to promote partial oxidation of CH_4 to produce an adsorbed methoxy species which can be desorbed in the form of methanol by using steam [2]. Various experimental and theoretical studies have been conducted to analyze the formation of dinuclear and trinuclear Cu-oxo clusters as CH_4 activating species [3] and to establish structure-activity relationships between formed Cu-oxo clusters and the nature of the activation process [4–6]. Fe-zeolites have also been explored as catalysts for the hydroxylation of CH_4 by the oxidants H_2O_2 [7] and N_2O [8,9], and dinuclear and mononuclear Fe-oxo ions are proposed to function as active sites. Recently, a ZSM-5-supported Rh catalyst was developed for catalytic oxidation of CH_4 in the presence of both O_2 and CO to form acetic acid and methanol [10]. Other zeolite-supported metal(-oxo) species, including those of Co, Ni, Au, and Ag, have been subjected to experimental and theoretical studies in order to evaluate their use in CH_4 activation under mild conditions [5,11–14]. In contrast to the large number of investigations carried out to date on transition metal incorporated systems, efforts focusing on main-group metal catalyst loaded zeolites for CH_4 activation are rare.

Since the 1990s, Ga-exchanged zeolites have been shown to be capable of activating low molecular weight alkanes and have been applied industrially as efficient catalysts for the dehydrocyclodimerization (DHCD) of propane to form aromatic compounds (Cyclar process) [15–17]. Ono *et al*. investigated the use of Ga-exchanged ZSM-5, prepared by using the liquid phase ion-exchange method, as a catalyst for dehydrocyclization reactions of light alkanes/alkenes at 773 K and discussed the mechanism of the process [18]. In a later investigation, Dooley *et al.* explored reductive solid-state ion-exchange (RSSIE) between Ga_2O_3 and proton-type ZSM-5 with the goal of improving catalytic activity by loading more Ga species in the zeolite [19,20]. Although identification of the form of Ga that is responsible for catalysis has been controversial, it has been proposed that Ga^+ and Ga-hydride ions are active species [21]. In the 2000s, Hensen *et al.* demonstrated by using infrared (IR)

spectroscopy that Ga-hydride species are formed on zeolites after RSSIE [15] and employed DFT calculations to describe the mechanism of dehydrogenation and oligomerization on this species [22–25]. Following these efforts, several groups demonstrated that Ga-hydride species, such as $[GaH_2]^+$ and $[GaH]^{2+}$, are active sites by employing a combination of experimental and theoretical methods [26–28]. Hensen *et al.* also observed in 2007 an acceleration effect of water on Ga-ZSM-5 catalyzed dehydrogenation reactions of alkanes [29] and then on the basis of the results of a theoretical study proposed that dinuclear Ga-oxo clusters are active species [30,31]. A selective catalytic reduction of NO_x with CH_4 (573-873 K) using Ga-exchanged zeolites was investigated by Kikuchi *et al.* [32]. By using an H/D exchange process, Stepanov *et al.* explored the ability of Ga-exchanged BEA zeolites to activate CH_4 at lower temperatures (423-563 K) [33]. A theoretical study of $[Ga=O]^+$ ion in ZSM-5 has also been carried out by Miyamoto *et al.* [34] Although many investigations of Ga-zeolite catalyzed activation/transformation of light alkanes including CH_4 have been conducted, thus far none have led to the development of methods for promoting these processes at room temperature.

Recently, we found that O_2 treatment for Indium (In)-exchanged CHA zeolite generates multinuclear In-oxo clusters, which promote oxidation of CH_4 at room temperature to form formic acid [35]. Encouraged by the results of this early study and the thought that Ga-zeolites can be employed for C−H activation, we designed an investigation aimed at the synthesis of Ga-oxo clusters in CHA zeolites (GaO_x-CHA) and an assessment of their ability to induce oxidation of CH_4 at room temperature. As described below, in the effort we demonstrated by using Ga K-edge XAFS that O_2 treatment of a RSSIE prepared Ga-exchanged zeolite forms a Ga-oxo cluster. *Ab initio* thermodynamic analysis was also carried out to gain information about plausible structures of the Ga-oxo species that exist in GaO_x-CHA at various temperatures. By using Fourier transform (FT)-IR spectroscopy, we showed that reaction of CH_4 promoted by zeolite-supported Ga-oxo clusters at room temperature generates adsorbed formaldehyde and formic acid. The mechanism of C–H bond cleavage in CH_4 was explored by using DFT calculations to evaluate possible transition states (TS) for the process.

2. Experimental and Methodology

2.1 Preparation of Ga-modified CHA zeolites

The preparation of GaO_x-CHA was conducted through impregnation of Ga species, RSSIE with H_2, and O_2 treatment. Specifically, a 1.0 g of CHA zeolite (Tosoh, NH_4^+-type, SiO_2/Al_2O_3 = 22.3, NH_4-CHA) and a 0.142 g of $Ga(NO_3)_3 \bullet nH_2O$ (n = 7-9, Wako) were added to 50 mL of deionized water (Ga/Al = ca. 0.4). The mixture was stirred, and the water was removed in vacuo. The resulting solid was dried in an oven and calcined at 773 K under an air atmosphere for 1 h, giving gallium oxide-modified CHA zeolite (denoted as Ga_2O_3/CHA). For RSSIE, Ga_2O_3/CHA was treated under a H_2 flow (20 $mLmin^{-1}$) at 973 K for 30 min to form Ga-exchanged CHA zeolite (denoted as Ga-CHA). O_2 treatment of Ga-CHA was carried out under an O_2 flow (20 $mLmin^{-1}$) at 773 K for 30 min to produce O_2-treated Ga-CHA (GaO_x-CHA) as a white powder.

2.2 Characterization

A temperature programmed reaction using H_2 (H_2-TPR) was performed with BELCAT II (MicrotracBEL). Ga_2O_3/CHA (ca. 50 mg) was pretreated at 773 K for 1 h and under a He atmosphere and then cooled to 373 K. The gas flow was switched to 5% H_2/Ar (30 $mLmin^{-1}$) while a thermal conductive detector was employed to observe H_2 consumption. A Ga K-edge XAFS measurement was conducted in the transmission mode in a BL14B2 station attached to a Si(311) monochromator at SPring-8 (JASRI), Japan (Proposal Nos. 2018B1768 and 2019A1614). The flow reaction system containing a flow-type cell was used for *in situ* XAFS measurements. Comparison of X-ray absorption near-edge structure (XANES) spectra was made using Athena (Demeter 0.9.26) while extended X-ray absorption fine structure (EXAFS) spectra were analyzed using the REX ver. 2.5 program (RIGAKU). Curve-fitting analysis was carried out using the parameters for the Ga–O and Ga–(O)–Ga shells provided by Mckale [36].

2.3 FT-IR spectroscopic monitoring of room temperature activation of CH_4 on GaO_x-CHA

FT-IR spectroscopy was conducted using a JASCO FT/IR-4600 spectrometer equipped with a triglycine sulfate (TGS) detector. A flow-type IR cell connected to a flow reaction system was used.

The powder sample of Ga_2O_3/CHA (40 mg) was subjected to a H_2 flow at 973 K for 30 min, and then set in the IR cell after pelletizing. The pellet was subjected to an O_2 flow (10% balanced with N_2, 100 $mLmin^{-1}$) at 773 K, prior to measurement of a background spectrum under a N_2 flow (90 $mLmin^{-1}$) at 303 K. A CH_4 flow (10% balanced with N_2, 100 $mLmin^{-1}$) was introduced to the IR cell after beginning continuous IR measurements. β-Ga_2O_3 was obtained by calcination of $Ga(NO_3)_3$•nH_2O at 1073 K for 4 h. α-Ga_2O_3 was prepared by calcination of commercially supplied gallium hydroxide (Mitsuwa Chemicals) at 823 K for 4 h [37].

2.4 DFT Calculations

DFT calculations were carried out using the periodic boundary condition under the Kohn–Sham formulation [38,39] as implemented in the Vienna ab-initio simulation package (VASP) [40,41]. The projected augmented waves (PAW) method was employed for the Kohn-Sham equations [42,43]. All atoms were allowed to fully relax during calculations and Spin-polarization was taken into account in all calculations. Electron exchange-correlation was treated by using the generalized gradient approximated Perdew-Burke-Ernzerhof (GGA-PBE) functional [44]. The plane basis set with a cut-off energy of 500 eV was used. The Γ point was used for Brillouin zone sampling. The semi-empirical Grimme's D3 method was employed to consider van der Waals (vdW) dispersion corrections [45,46]. During the calculations, the lattice constants of CHA zeolite were fixed at values given in the International Zeolite Association (IZA) database (a = b = 13.675 Å, c = 14.767 Å, α = β = 90.0° and γ = 120°) [47]. Three paired Al sites (Z_2, an Al site is denoted as Z) in CHA are considered as a third-nearest-neighbor site in a six-membered-ring (6MR(3NN)), and a third-nearest-neighbor site and a fourth-nearest-neighbor site in an eight-membered ring (8MR(3NN) and 8MR(4NN), respectively). The unit cell of CHA zeolite along with these paired Al sites are illustrated in Fig. 1.

Ab initio thermodynamic analysis was applied to consider the effect of O_2, water and temperature on Ga-oxo ions in CHA zeolites [48]. Enthalpies and entropies at each temperature, and the standard state pressure (0.1 MPa) were obtained from NIST-JANAF Thermochemical Tables [49]. The following equilibrium reaction was considered;

$$\mathrm{xGaOH/CHA} + (1-\mathrm{x})\mathrm{CHA\_2H} + \frac{(2\mathrm{m}-3\mathrm{x}-\mathrm{n}+2)}{4}\mathrm{O_2} + \frac{(\mathrm{x}+\mathrm{n}-2)}{2}\mathrm{H_2O} \leftrightharpoons \mathrm{Ga_xO_mH_n/CHA} \quad (1)$$

where the reaction energy is denoted as

$$\Delta E = E_{Ga_xO_mH_n/CHA} - xE_{GaOH/CHA} - (1-x)E_{CHA\_2H} - \frac{(2m-3x-n+2)}{4}E_{O_2} - \frac{(x+n-2)}{2}E_{H_2O} \quad (2)$$

In this way, $E_{Ga_xO_mH_n/CHA}$ represents the total energy of the CHA zeolite model containing Ga-oxo ions. $E_{GaOH/CHA}$ is that of the Ga-CHA model containing Z_2[GaOH] (Z_2[GaOH] denotes the $[GaOH]^{2+}$ ion on paired Al site). E_{CHA_2H}, E_{O_2} and E_{H_2O} represent the total energies of the unit cell of CHA zeolite possessing two protons for charge compensation, gaseous water, and oxygen molecules, respectively. The Gibbs free energy ΔG is given as

$$\Delta G(T,p) = \frac{1}{A}\left[\Delta E - \frac{(2m-3x-n+2)}{2}\Delta\mu_O - \frac{(x+n-2)}{2}\Delta\mu_{H_2O}\right] \quad (3)$$

A represents the area of the unit cell. The change of chemical potential $\Delta\mu$ is defined as

$$\Delta\mu_O(T,p) = \frac{1}{2}\left[\Delta\mu_{O_2}(T,p^0) + RT\,ln\left(\frac{p_{O_2}}{p^0}\right)\right] \quad (4)$$

$$\Delta\mu_{H_2O}(T,p) = \Delta\mu_{H_2O}(T,p^0) + RT\,ln\left(\frac{p_{H_2O}}{p^0}\right) \quad (5)$$

The conjugate gradient method was used to optimize intermediate structures during the climbing-image Nudge elastic band (CI-NEB) calculations as implemented in VTST-Tools [50]. Once the maximum forces on all atoms are less than 0.03 and 0.05 eV $Å^{-1}$, the geometry optimizations and CI-NEB calculations are considered converged, respectively. For CI-NEB calculations, a 400 eV cut-off energy was employed to reduce the computational cost. The spring constant between adjacent images was set to 5.0 eV/$Å^2$. All structure graphics were generated by using visual molecular dynamics software (VMD) [51].

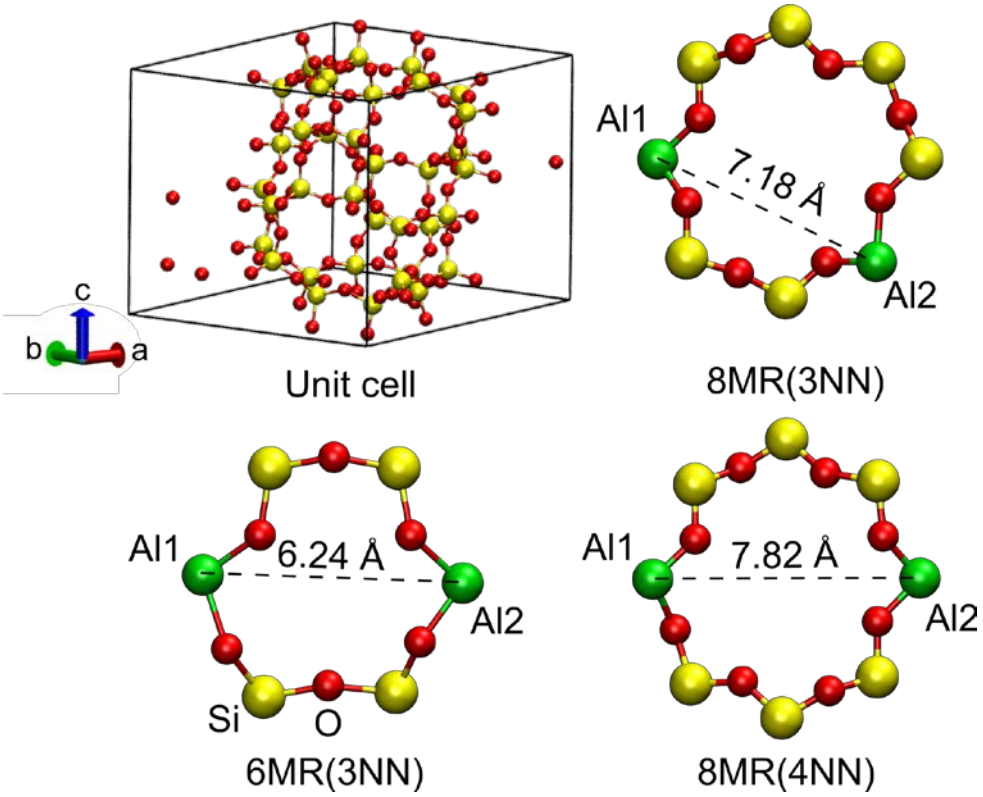

Fig. 1 Unit cell of CHA zeolite and paired Al sites investigated in periodic DFT calculations. Yellow: Si, Red: O, and Green: Al.

3. Results and Discussion

3.1 XAFS and H_2-TPR measurements

GaO_x-CHA was prepared by calcination (773 K) of a mixture of $Ga(NO_3)_3$ and NH_4-CHA, obtained by impregnation, followed by sequential RSSIE with H_2 (973 K) and O_2 treatment (773 K). To trace the redox characteristics of Ga species formed during preparation of GaO_x-CHA, Ga K-edge XANES spectroscopic analysis was performed. Normalized XANES spectra of a sample of Ga-modified CHA zeolites at different points in the preparative sequence, along with those of reference samples (β-Ga_2O_3 and $Ga(acac)_3$, acac denotes acetylacetonate) are displayed in Fig. 2(a). It is well-known that XANES spectra of gallium oxides contain two distinguishable peaks assignable to respective octahedral and tetrahedral Ga^{3+} species [37,52]. The XANES spectrum of β-Ga_2O_3, which contains both of these Ga^{3+} species, contains an absorption maximum at 10376 eV and a shoulder around 10373 eV, while one narrow peak at 10376 eV exists in the spectrum of $Ga(acac)_3$. The spectrum of Ga_2O_3/CHA following calcination contains the two characteristic absorption peaks corresponding to octahedral and tetrahedral Ga^{3+} species. Upon H_2 treatment of the calcinated sample at 973 K, the absorption edge shifts to lower energy by 4-5 eV (Ga-CHA), indicating that reduction of Ga species by H_2 occurs during RSSIE. This conclusion is supported by H_2-TPR, which showed that consumption peak for H_2 is generated from 873 to 973 K (Fig. 3). Also, *in situ* XANES measurements were carried out on a sample subjected to a 5% H_2/He flow at 973 K. The *in situ* XANES spectra and corresponding ΔXANES spectra, obtained by subtraction of the spectrum of Ga_2O_3/CHA at the beginning of H_2 treatment at room temperature (298 K), are given in Fig. 2(c) and (d), respectively. The data show that the broad peak at 10373 eV in the ΔXANES spectrum disappears in concert with the appearance of another narrow peak at 10368 eV. The observed shift in the absorption edge in the ΔXANES spectrum is nearly the same as those observed by Hock et al [53] for H_2 reduction of Ga-modified BEA zeolite, and rationalized to correspond to formation of a $[GaH_2]^+$ ion from gallium oxide via a $[GaH]^{2+}$ ion. Thus, it appears that a similar phenomenon is occurring with the CHA zeolite.

Upon exposure to O_2 at 773 K, the absorption edge shifts to higher energy in a manner that is similar to that of β-Ga_2O_3, and spectrum contains mainly one peak associated with tetrahedral Ga. These results suggest that a Ga-oxo species different from Ga_2O_3 is produced. To gain more insight into the

nature of the Ga-oxo species formed in the above process, extended XAFS (EXAFS) spectra were analyzed for β-Ga_2O_3 and GaO_x-CHA at room temperature (Fig. 2(b)). The FT-EXAFS spectrum of GaO_x-CHA, which is different from that of β-Ga_2O_3, contains two peaks which correspond to Ga–O and Ga−(O)–Ga shells. The intensity of a peak derived from Ga−(O)–Ga shell for GaO_x-CHA was lower than that for β-Ga_2O_3. The results of curve-fitting analysis show that the coordination number (CN) and interatomic distance (R) of the Ga−(O)−Ga shell are 1.06 and 2.96 Å, respectively (Table 1). Based on these findings, we conclude that a Ga-oxo cluster is generated in CHA zeolite by O_2 treatment of Ga-exchanged CHA, prepared by using RSSIE.

Table 1. Results of curve-fitting analysis of Ga K-edge EXAFS of GaO_x-CHA

Shell	CN[a]	R[b] (Å)	ΔE[c] (eV)	σ[d] (Å)	R[e] (%)
Ga−O	4.82 ± 1.04	1.90 ± 0.02	6.11	0.11	0.60
Ga−(O)–Ga	1.06 ± 0.84	2.96 ± 0.05	-8.07	0.08	-

[a] Coordination number. [b] Bond distance. [c] Increase in the threshold energy. [d] Debye–Waller factor. [e] Residual factor.

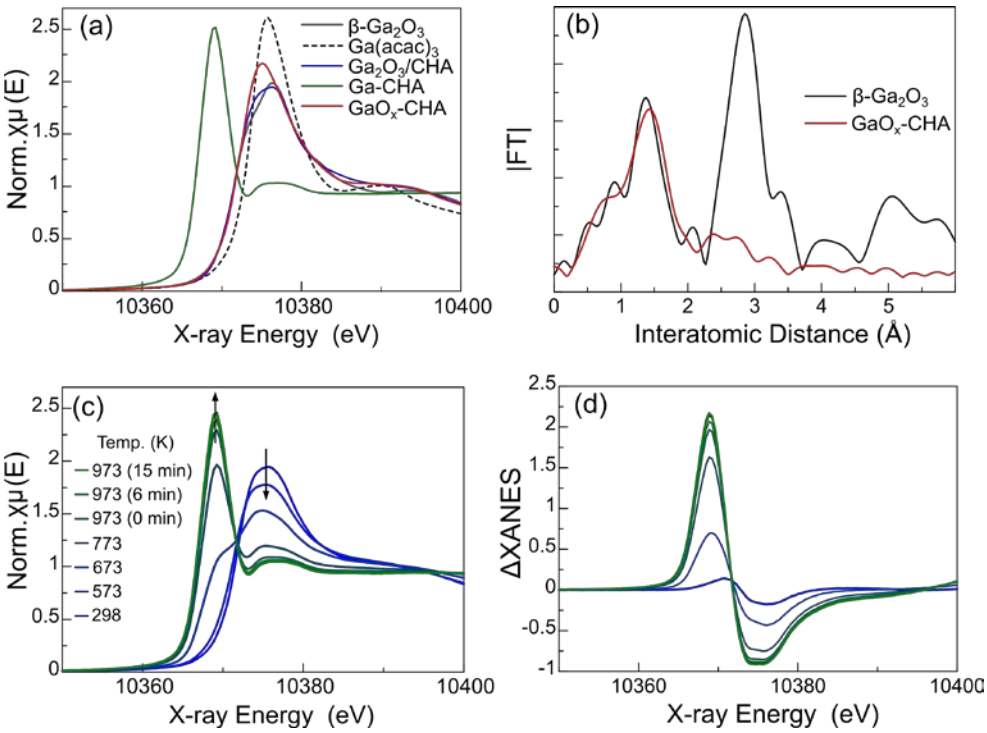

Fig. 2 (a) Normalized Ga K-edge XANES spectra of β-Ga_2O_3, $Ga(acac)_3$, Ga_2O_3/CHA, Ga-CHA (after H_2 treatment of Ga_2O_3/CHA at 973 K), GaO_x-CHA (after O_2 treatment of Ga-CHA at 773 K). (b) FT of k^3-weighted EXAFS oscillations measured at room temperature for β-Ga_2O_3 and GaO_x-CHA. (c) *In situ* Ga K-edge XANES spectra during H_2 treatment of Ga_2O_3/CHA. (d) Corresponding ΔXANES spectra obtained by subtraction of the spectrum of Ga_2O_3/CHA at the beginning of H_2 treatment at room temperature (298 K).

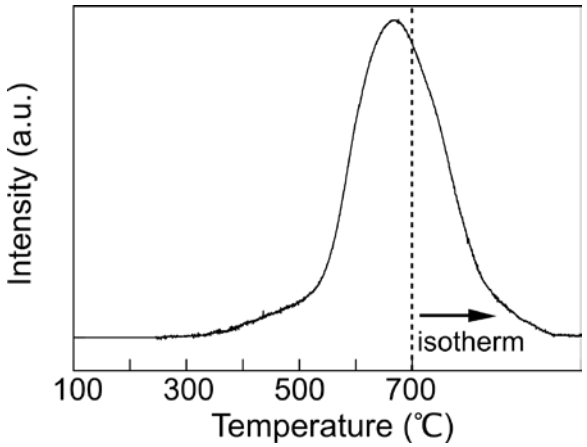

Fig. 3 H_2-TPR profile of Ga_2O_3/CHA under H_2 flow.

3.2 *Ab initio* thermodynamic analysis

An *ab initio* thermodynamic approach was carried out to gain information about plausible structures of the Ga-oxo species in GaO_x-CHA [54,55]. This method has been applied to the analysis of stabilities of multinuclear metal-oxo clusters, such as those of Cu, Al, and Fe, in zeolites [48,56,57]. The relative Gibbs free energies of various Ga-oxo ions at possible coordination sites as a function of O_2 chemical potential and temperature were calculated. For this purpose, the chemical potential of water was fixed so that the corresponding partial pressure is 0.001 atm (dehydration conditions). Three kinds of paired Al sites, 6MR(3NN), 8MR(3NN), and 8MR(4NN) (Fig.1), were considered as coordination sites in CHA. The feasibility of these models was validated by recent theoretical works describing paired Al sites to accommodate cationic species [58,59] and experimental works investigating the presence of paired Al sites [60,61]. The calculated free energies for the formation of Ga-oxo ions ((a)-(c)) and a phase diagram predicting which of the Ga(-oxo) ion on paired Al sites (Z_2) is the most thermodynamically stable ((d)–(f)) are given in Fig. 4. O_2 chemical potentials were translated into the O_2 partial pressures, denoted as $\log(p_{O2})$. The phase diagram obtained for 6MR(3NN) (Fig. 4(d)) shows that $Z_2[Ga_2(OH)_4]$ dimer is the lowest energy Ga-oxo species below 300 K and that Z_2[GaOH] monomer is the most stable one at higher temperatures. In the case of 8MR(3NN) (Fig. 4(e)), the most stable species in the lower temperature region is $Z_2[Ga_2(OH)_4]$ dimer, however, $Z_2[Ga_2O_2]$ dimer rather than Z_2[GaOH] monomer is the lowest energy species as the temperature rises from 400 K to 600 K. It is also predicted that thermal reduction of $Z_2[Ga_2O_2]$ to form the Ga^+ cation occurs at higher temperature (1200 K) and very low p_{O2} ($< 1\times10^{-6}$ atm). The existence of similar dinuclear $[Ga_2O_2]^{2+}$ ions in other zeolites was proposed by Hensen et al [30]. Finally, in the case of 8MR(4NN) (Fig. 4(f)), the nature of the lowest energy ion dependencies on $\log(p_{O2})$ and temperature are similar to those in 8MR(3NN), although the temperature region over which $Z_2[Ga_2O_2]$ exists is wider (450-1200 K).

The calculated relative energies of other Ga-oxo clusters, such as $Z_2[Ga_2(O)(OH)_2]$, $Z_2[Ga_2O_2]$ and $Z_2[Ga_3(O)_2(OH)_3]$, at $\log(p_{O2}) = 0.1$ and 300 K were compared to the corresponding XAFS data for a sample treated with 10% O_2 at 773 K followed by cooling to room temperature. Fig. 4(g) shows the relative energies of Ga(-oxo) ions on each paired Al site with respect to the lowest-energy Ga-oxo ions. At 6MR(3NN), $Z_2[Ga_2(OH)_4]$ has a lower relative energy (ca. 0.1 eV), compared to those of other

Ga-oxo clusters (>ca. 0.65 eV). In the case of 8MR(3NN), Z_2[GaOH] has the second lowest relative energy (ca. 0.5 eV) and the relative energies of other clusters are higher (ca. 0.7-0.8 eV). In contrast, at 8MR(4NN), $Z_2[Ga_2(O)(OH)_2]$, $Z_2[Ga_2O_2]$, and $Z_2[Ga_3(O)_2(OH)_3]$, have lower relative energies (ca. 0.25 to 0.6 eV). Note that higher oligomers, such as $Z_2[Ga_4O_4]$, have much higher relative energies (>ca. 1.4 eV) at all paired Al sites. Based on these results, it is predicted that Ga-oxo clusters, such as the $Z_2[Ga_2(O)(OH)_2]$, $Z_2[Ga_2O_2]$, and $Z_2[Ga_3(O)_2(OH)_3]$, are likely to be present at 8MR(4NN) rather than 8MR(3NN), and 6MR(3NN). One of the main reasons for this is that, among the paired Al sites in CHA (Fig. 1), the longest Al−Al distance exists in 8MR(4NN). Thus, 8MR(4NN) has larger space compared to that of 8MR(3NN), and 6MR(3NN), which can effectively stabilize multinuclear metal cations. Additionally, we investigated p_{H2O} dependency of calculated relative Gibbs free energies of Ga-oxo species (Fig. 5). $Z_2[Ga_2(OH)_4]$ and $Z_2[Ga_3(O)_2(OH)_3]$ become thermodynamically more stable rather than $Z_2[Ga_2(O)(OH)_2]$ with the increase of p_{H2O}. In the theoretical study of CH_4 activation (see below), we consider Z_2[GaOH] at 6MR(3NN) to be a monomer model and $Z_2[Ga_2(O)(OH)_2]$, $Z_2[Ga_2(OH)_4]$, $Z_2[Ga_2O_2]$, and $Z_2[Ga_3(O)_2(OH)_3]$ at 8MR(4NN) to be cluster models (Fig. 6).

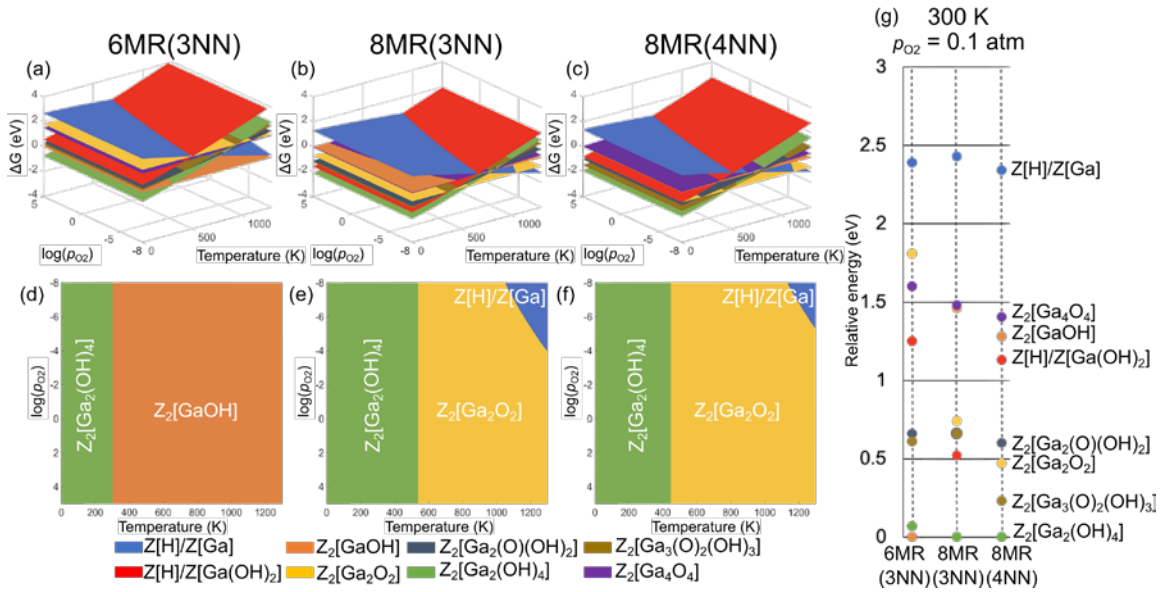

Fig. 4 Free energy (ΔG) for the formation of the Ga(-oxo) ions on paired Al sites (Z_2) in CHA (top) and phase diagram showing the lowest-energy species (bottom) as a function of O_2 partial pressure ($\log(p_{O2})$) and temperature on (a and d) 8MR(4NN), (b and e) 8MR(3NN), and (c and f) 6MR(3NN). (g) Relative energies of Ga(-oxo) ions at each paired Al sites, referenced to the lowest-energy Ga-oxo ions, O_2 partial pressure: 0.1 atm, Temperature: 300 K.

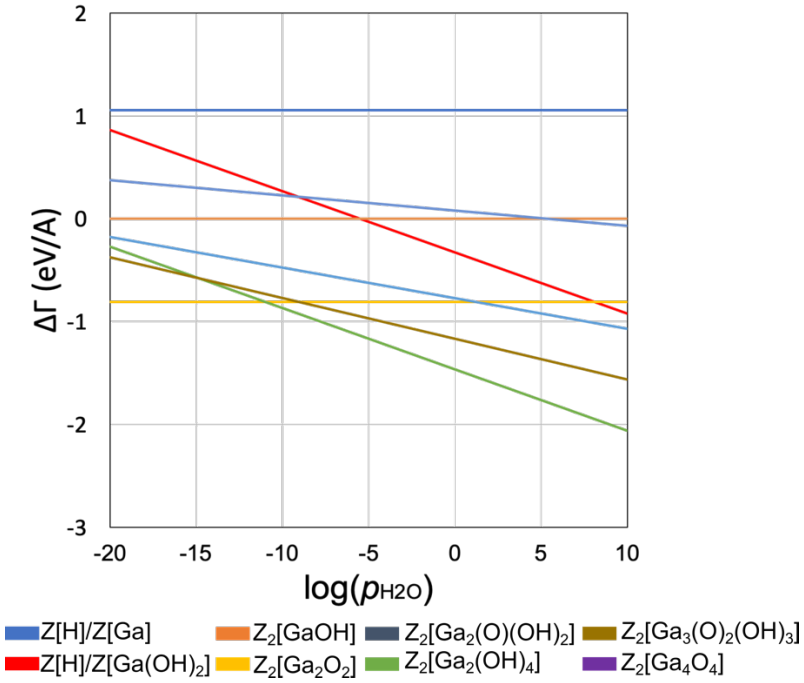

Fig. 5 Calculated relative Gibbs free energies (ΔG) of Ga-oxo species at 8MR4NN in CHA zeolite as a function of partial pressure of water (log(pH$_2$O)) at 300 K.

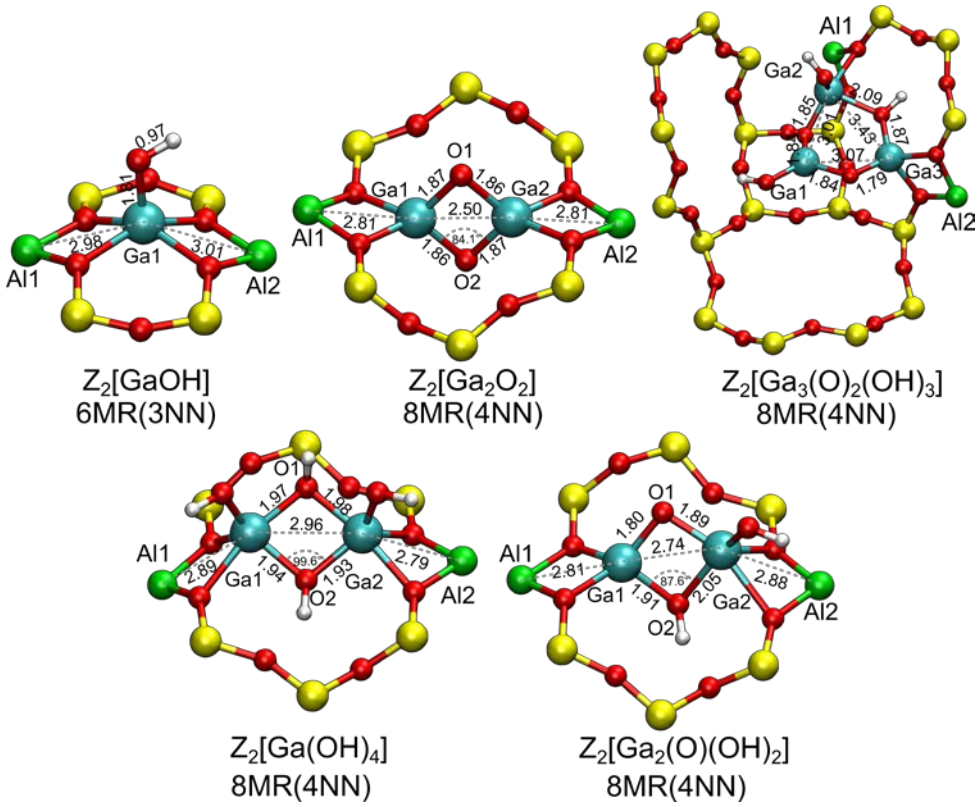

Fig. 6 Plausible Ga-oxo species on paired Al sites in CHA zeolite.

3.3 Experimental and theoretical studies probing CH_4 activation at low temperature

Although various experimental and theoretical studies have been conducted, the activation/transformation of the highly stable C−H bond in CH_4 at low temperatures remains a formidable task [56-66]. As mentioned in the Introduction, we recently showed that CHA zeolite-supported In-oxo clusters promotes oxidation of CH_4 at room temperature to form adsorbed formic acid. To evaluate the abilities of Ga-oxo clusters to activate CH_4, *in situ* FT-IR analysis was carried out on a CH_4 flow in the presence of GaO_x-CHA zeolites at room temperature (Fig. 7). After purging with CH_4 for 100 min followed by N_2 purging, the GaO_x-CHA zeolite was found to display one narrow FT-IR peak at 1490 cm^{-1} and two peaks around 1700 and 1400 cm^{-1}. The peak at 1490 cm^{-1} is assignable to scissoring of surface dioxymethylene species (–OCH_2O–), which correspond to adsorbed formaldehyde [73]. Deconvolution of the peak around 1700 cm^{-1} revealed that it is composed of three peaks at 1719, 1644 and 1609 cm^{-1}, which correspond to C=O stretching of H-bonded HCO_2H, Lewis-acid coordinated HCO_2H and water, respectively [74]. The band at ca. 1400 cm^{-1} can also be deconvoluted into two peaks at 1377 and 1413 cm^{-1}, which are attributable to respective C–H bending of adsorbed HCO_2H and waging of surface –OCH_2O– groups, respectively [74]. The above peaks do not appear in FT-IR spectra recorded on a CH_4 flow over bulk oxides such as β-Ga_2O_3 and α-Ga_2O_3. The absorbance derived from the adsorbed oxygenates decreased with the decrease of Ga loading while the similar IR spectrum was obtained using the GaO_x-CHA with higher Ga loading (Fig. S1). The formation of formaldehyde and formic acid was supported by the FT-IR measurement after adsorption of 1,3,5-trioxane (as a synthon of formaldehyde) and formic acid on GaO_x-CHA and H-CHA as shown in Fig. S2. The reaction of CH_4 in the presence of water vapor was also carried out using a bubbler filled with water, but any products were not obtained. In the presence of water, active Ga-oxo clusters might be converted to less active ones (see below). Furthermore, we tried to extract the adsorbed products using D_2O and then to evaluate their amounts by ^1H NMR. Unfortunately, any product was not detected, which would be due to the difficulty of extraction from small pores of CHA zeolites. The combined results show that CH_4 undergoes oxidation at room temperature over Ga-oxo clusters in CHA zeolite to produce adsorbed formic acid and formaldehyde. This process is different from CH_4 oxidation by InO_x-CHA where only adsorbed formic acid is produced.

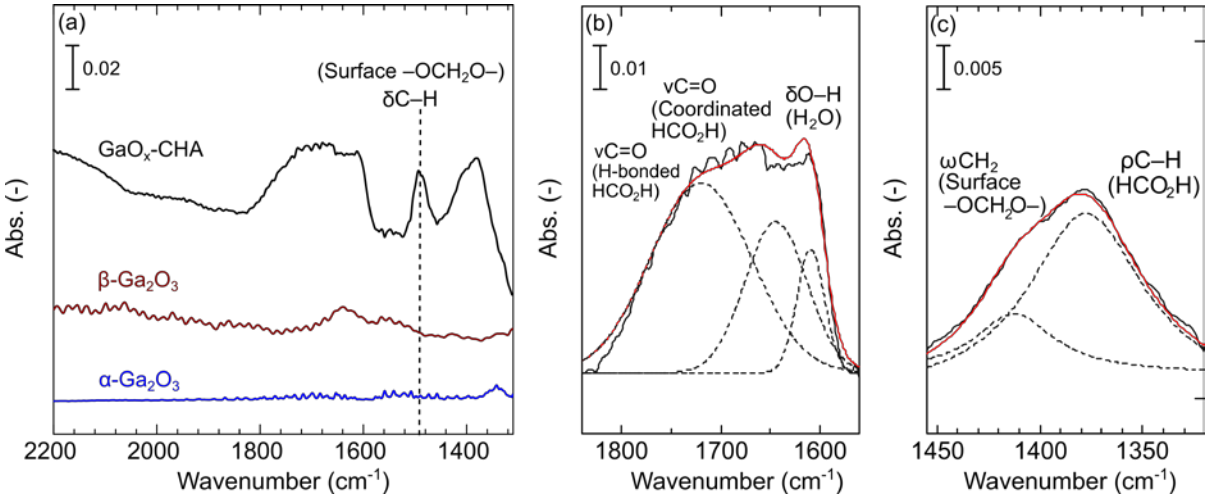

Fig. 7 (a) FT-IR spectra during reaction of CH_4 over GaO_x-CHA at room temperature. Deconvolution of the bands around (b) 1700 cm^{-1} and (c) 1400 cm^{-1}.

The mechanism for oxidation of CH_4 promoted by Ga-oxo clusters in CHA zeolite was explored by employing DFT calculations to evaluate possible transition states (TSs) for C–H bond cleavage, which is considered to be the rate-determining step in the process [71]. For this purpose, DFT calculations, using the periodic boundary condition in the Kohn–Sham formulation [38,39] as implemented in VASP [40,41], were performed to obtain activation barriers for the C–H bond cleavage in plausible models, including Ga-oxo monomer (Z_2[GaOH] at 6MR(3NN)) and clusters ($Z_2[Ga_2O_2]$, $Z_2[Ga_2(OH)_4]$, $Z_2[Ga_2(O)(OH)_2]$, and $Z_2[Ga_3(O)_2(OH)_3]$ at 8MR(4NN)). The TS structures for the C–H bond cleavage step (Fig. 8) and the corresponding energy diagrams (Fig. 9) are displayed. The CH_4 adsorption energies for the Ga-oxo clusters are calculated to be in the range of -24.4 to -26.3 kJ/mol while that for Z_2[GaOH] is slightly lower (-22.5 kJ/mol). The energies for absorption of CH_4 to the Ga-oxo clusters are much lower than those to In-oxo clusters (ca. -40 kJ/mol, given in our previous publication [35]). In the context of geometric parameters, the Ga−C bond distances and H−C−H angles directed to Ga cations are calculated to be ca. 3.26-4.78 Å and 109-110˚, respectively. These values are smaller than those for In-oxo clusters (2.87-2.91 Å and 112-114˚, respectively [34]), an observation that is consistent with the lower adsorption energies of Ga-oxo clusters.

Following adsorption of CH_4, Ga-oxo species promote cleavage of the C–H bond. Among those induced by Ga-oxo species evaluated in this effort, the C–H bond cleavage reaction promoted by

$Z_2[Ga_2(O)(OH)_2]$ has the lowest calculated energy barrier (E_a = 96.8 kJ/mol). The respective activation barriers for processes induced by $Z_2[Ga_2(OH)_4]$ and $Z_2[Ga_3(O)_2(OH)_3]$ are 135.5 and 139.8 kJ/mol, and that for the $Z_2[Ga_2O_2]$-catalyzed reaction is much higher than those of the other Ga-oxo clusters. Monomeric $Z_2[GaOH]$ has the highest E_a (175.2 kJ/mol), which is about twice that of the C–H bond rupture step promoted by $Z_2[Ga_2(O)(OH)_2]$. Following cleavage of the C−H bond in CH_4, a Ga−CH_3 intermediate with Ga−C bond distances of 1.96 Å are formed from all Ga-oxo species. In the cases of $Z_2[Ga_2O_2]$, $Z_2[Ga_2(O)(OH)_2]$, and $Z_2[Ga_3(O)_2(OH)_3]$ an O−H bond is formed through reaction of a bridging O atom with a H atom derived from CH_4, and in the $Z_2[Ga_2(OH)_4]$ and $Z_2[GaOH]$ promoted processes the H atom derived from CH_4 reacts with the OH ligand to form water. The C−H bond cleavage reactions catalyzed by the Ga-oxo species are calculated to be exothermic (-15.5 to -136.8 kJ/mol) except for reaction promoted by $Z_2[Ga_2(OH)_4]$ which is endothermic (ΔE = 1.18 kJ/mol). Based on the above results, it appears that CH_4 weakly adsorbs to all Ga-oxo species regardless of their structure and nuclearilty and that C−H bond cleavage in CH_4 occurs most efficiently on $Z_2[Ga_2(O)(OH)_2]$. The loss of activity of GaO_x-CHA for CH_4 activation in the presence of water vapor is interpreted as the conversion of the most active $Z_2[Ga_2(O)(OH)_2]$ into less active species such as $Z_2[Ga_2(OH)_4]$ and $Z_2[Ga_3(O)_2(OH)_3]$, which was indicated by the p_{H2O} dependency of calculated relative Gibbs free energies of Ga-oxo species (Fig. 5).

The mechanism of C−H bond cleavage on $Z_2[Ga_2(O)(OH)_2]$ was subjected to further investigation. It is reported that zeolite-supported transition metal catalyst clusters cleave C−H bonds of light alkanes in a homolytic manner (Cu, Fe, Ni) [8,75–77] while cleavage of C−H bonds occurs heterolytically on main-group metal species (In, Ga) in zeolites [35,78,79]. The results of calculations on the process promoted by $Z_2[Ga_2(O)(OH)_2]$ show that the energy of the intermediate methyl radical is two-times larger (188.8 kJ/mol) than the activation barrier for C–H bond heterolytic cleavage (96.5 kJ/mol, Fig. 10). This finding suggests that Ga-oxo induced cleavage of a C−H bond in CH_4 occurs heterolytically.

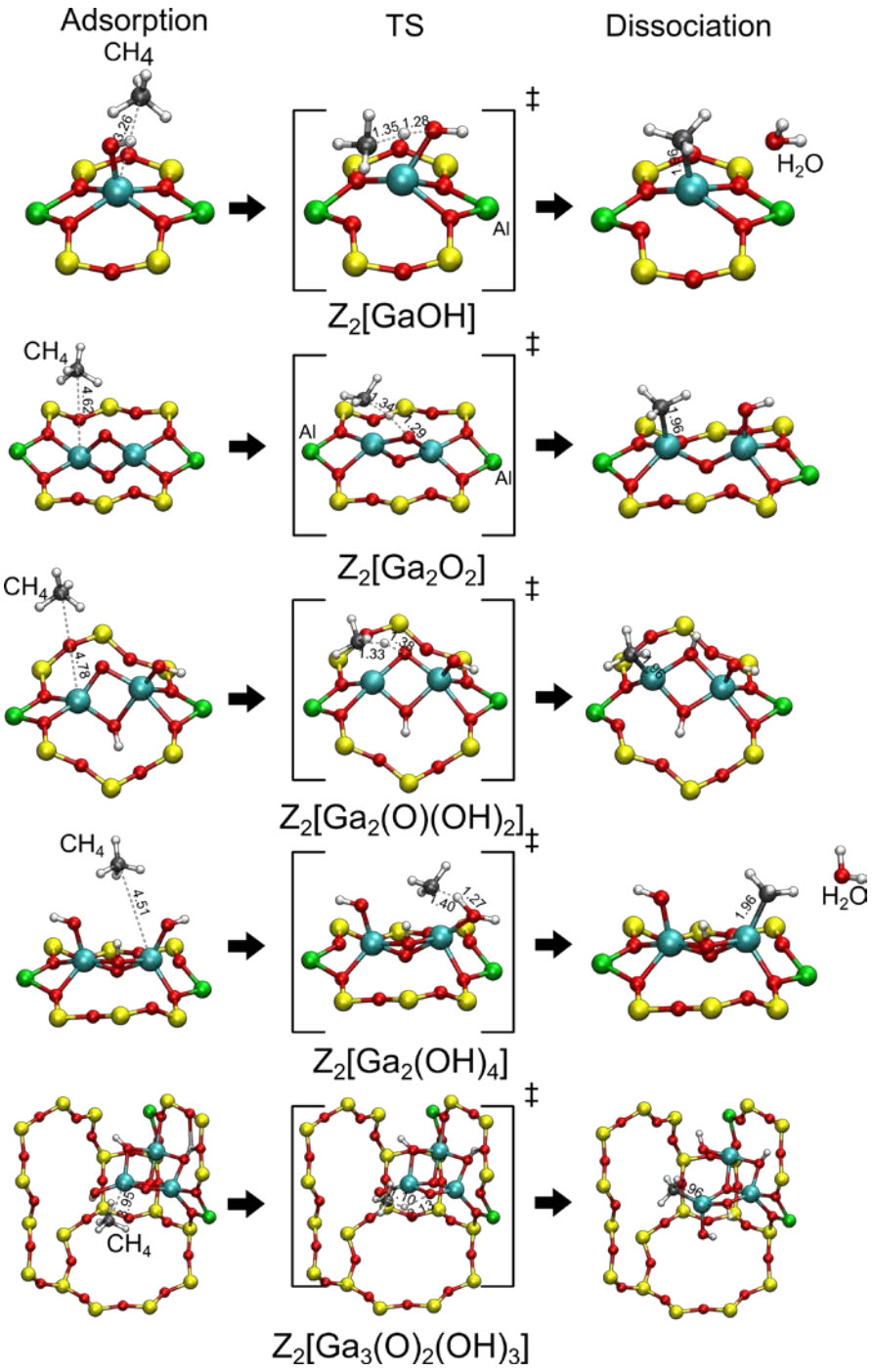

Fig. 8 Optimized DFT-calculated structures of intermediates and TSs for C–H cleavage of CH_4 promoted by monomer (Z_2[GaOH] at 6MR(3NN)) and clusters ($Z_2[Ga_2O_2]$, $Z_2[Ga_2(OH)_4]$, $Z_2[Ga_2(O)(OH)_2]$, and $Z_2[Ga_3(O)_2(OH)_3]$ at 8MR(4NN)) together.

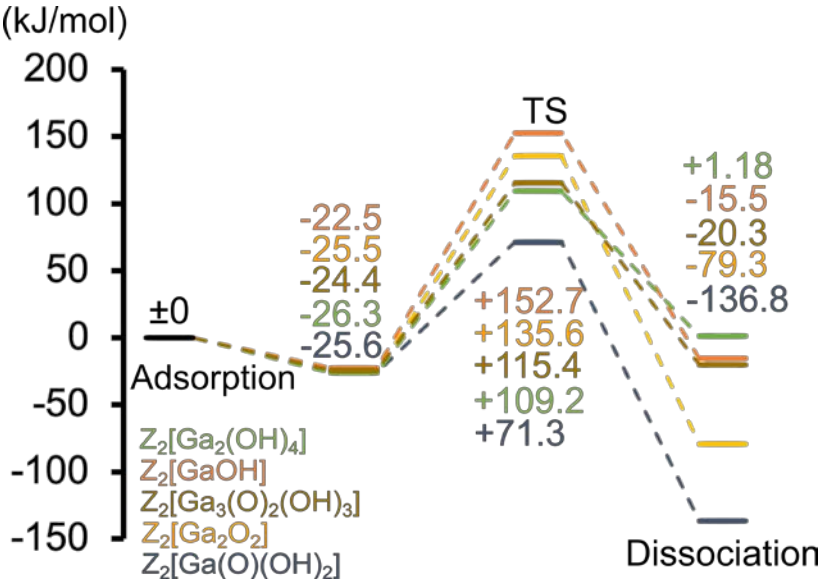

Fig. 9 DFT(PBE)-calculated energy diagrams of C–H bond cleavage reaction over predicted Ga-oxo species. Energies are given in kJ/mol and include the vdW-D3 dispersive correction.

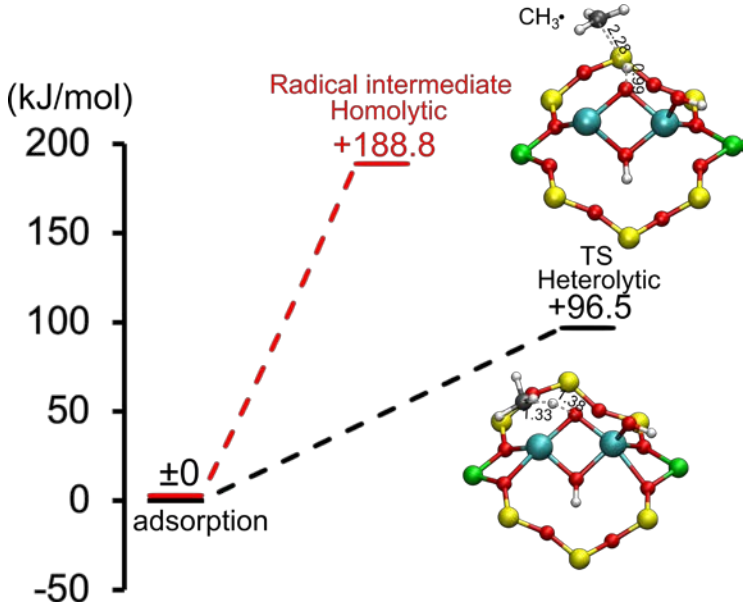

Fig. 10 Comparison of energy diagrams for C−H cleavage of CH_4 promoted by $Z_2[Ga_2O_2]$ at 8MR(4NN) occurring through heterolytic (black) and homolytic pathways (red).

Conclusion

In this investigation, we demonstrated that CH_4 oxidation at room temperatures is promoted by O_2-activated Ga-exchanged CHA zeolite. The results of *in situ* XAFS and H_2-TPR studies suggest that multinuclear Ga-oxo clusters are produced by sequential RSSIE (H_2, 973 K) and oxidation (O_2, 773 K). Possible structures of Ga-oxo clusters responsible for this process were explored by using *ab initio* thermodynamic analysis. The results suggest that the plausible active species are $Z_2[Ga_2O_2]$ $Z_2[Ga_2(OH)_4]$, $Z_2[Ga_2(O)(OH)_2]$, and $[Ga_3(O)_2(OH)_3]^{2+}$ under p_{O2} = 0.1 atm, dry conditions (p_{H2O} = 0.001 atm), and room temperature (300 K). The generation of adsorbed formic acid and formaldehyde in this process was demonstrated by using *in situ* IR spectroscopic monitoring of reaction of a CH_4 flow over Ga-oxo clusters in CHA zeolite at room temperature. The energy barriers for C–H bond cleavage over possible Ga-oxo species were calculated using DFT calculations. The results show that the process promoted by $Z_2[Ga_2(O)(OH)_2]$ ion has the lowest activation barrier. Finally, the results suggest that the C−H bond cleavage reaction promoted by Ga-oxo species proceeds through a heterolytic pathway rather than a homolytic pathway. Overall, this effort demonstrates the potential of using zeolite-supported main-group metal-oxo clusters as catalysts for CH_4 oxidation under mild conditions.

Acknowledgements

This study was supported financially by JSPS KAKENHI grants (17H01341, 18K14051 and 18K14057) from the Japan Society for the Promotion of Science (JSPS) and by the Japanese Ministry of Education, Culture, Sports, Science, and Technology (MEXT) within the projects "Integrated Research Consortium on Chemical Sciences (IRCCS)" and "Elements Strategy Initiative to Form Core Research Center", as well as by the JST-CREST projects JPMJCR17J3 and JPMJCR15P4. The authors are indebted to the technical division of the Institute for Catalysis (Hokkaido University) for manufacturing experimental equipment. XAFS measurements were performed at the BL14B2 facility of SPring-8 at the Japan Synchrotron Radiation Research Institute (JASRI) (Proposal Nos. 2018B1768 and 2019A1614).

Appendix A. Supplementary data Supplementary

Supplementary data associated with this article can be found,

in the online version, at

Reference

[1] P. Schwach, X. Pan, X. Bao, Chem. Rev. 117 (2017) 8497–8520.

[2] M.H. Groothaert, P.J. Smeets, B.F. Sels, P.A. Jacobs, R.A. Schoonheydt, J. Am. Chem. Soc. 127 (2005) 1394–1395.

[3] S. Grundner, M.A.C. Markovits, G. Li, M. Tromp, E.A. Pidko, E.J.M. Hensen, A. Jentys, M. Sanchez-Sanchez, J.A. Lercher, Nat. Commun. 6 (2015) 7546.

[4] C. Liu, G. Li, E.A. Pidko, Small Methods 2 (2018) 1800266.

[5] M.H. Mahyuddin, Y. Shiota, A. Staykov, K. Yoshizawa, Acc. Chem. Res. 51 (2018) 2382–2390.

[6] P. Vanelderen, B.E.R. Snyder, M.L. Tsai, R.G. Hadt, J. Vancauwenbergh, O. Coussens, R.A. Schoonheydt, B.F. Sels, E.I. Solomon, J. Am. Chem. Soc. 137 (2015) 6383–6392.

[7] P. Xiao, Y. Wang, T. Nishitoba, J.N. Kondo, T. Yokoi, Chem. Commun. 55 (2019) 2896–2899.

[8] B.E.R. Snyder, P. Vanelderen, M.L. Bols, S.D. Hallaert, L.H. Böttger, L. Ungur, K. Pierloot, R.A. Schoonheydt, B.F. Sels, E.I. Solomon, Nature 536 (2016) 317–321.

[9] M.H. Mahyuddin, Y. Shiota, A. Staykov, K. Yoshizawa, Inorg. Chem. 56 (2017) 10370–10380.

[10] J. Shan, M. Li, L.F. Allard, S. Lee, M. Flytzani-Stephanopoulos, Nature 551 (2017) 605–608.

[11] K. Nakamura, A. Okuda, K. Ohta, H. Matsubara, K. Okumura, K. Yamamoto, R. Itagaki, S. Suganuma, E. Tsuji, N. Katada, ChemCatChem 10 (2018) 4113–4119.

[12] G. Wang, L. Huang, W. Chen, J. Zhou, A. Zheng, Phys. Chem. Chem. Phys. 20 (2018) 26522–26531.

[13] S. Wannakao, C. Warakulwit, K. Kongpatpanich, M. Probst, J. Limtrakul, ACS Catal. 2 (2012) 986–992.

[14] T. Baba, H. Sawada, Phys. Chem. Chem. Phys. 4 (2002) 3919–3923.

[15] D. Seddon, Catal. Today 6 (1990) 351–372.

[16] N.Y. Chen, T.Y. Yan, Ind. Eng. Chem. Process Des. Dev. 25 (1986) 151–155.

[17] S.M. Al-Zahrani, Dev. Chem. Eng. Min. Process. 6 (2008) 101–120.

[18] H. Kitagawa, Y. Sendoda, Y. Ono, J. Catal. 101 (1986) 12–18.

[19] V. Kanazirev, G.L. Price, K.M. Dooley, Stud. Surf. Sci. Catal. 69 (1991) 277–285.

[20] K.M. Dooley, C. Chang, G.L. Price, Appl. Catal. A Gen. 84 (1992) 17–30.

[21] G.D. Meitzner, E. Iglesia, J.E. Baumgartner, E.S. Huang, J. Catal. 140 (1993) 209–225.

[22] V.B. Kazansky, I.R. Subbotina, R.A. van Santen, E.J.M. Hensen, J. Catal. 227 (2004) 263–269.

[23] V.B. Kazansky, I.R. Subbotina, R.A. Van Santen, E.J.M. Hensen, J. Catal. 233 (2005) 351–358.

[24] M. V. Frash, R.A. van Santen, J. Phys. Chem. A 104 (2000) 2468–2475.

[25] E.A. Pidko, E.J.M. Hensen, R.A.V. Santen, J. Phys. Chem. C 112 (2008) 19604–19611.

[26] M.S. Pereira, M.A.C. Nascimento, Chem. Phys. Lett. 406 (2005) 446–451.

[27] E. Mansoor, M. Head-Gordon, A.T. Bell, ACS Catal. 8 (2018) 6146–6162.

[28] C. Copéret, D.P. Estes, K. Larmier, K. Searles, Chem. Rev. 116 (2016) 8463–8505.

[29] E.J.M. Hensen, E.A. Pidko, N. Rane, R.A. Van Santen, Angew. Chem. Int. Ed. 46 (2007) 7273–7276.

[30] E.A. Pidko, R.A. Van Santen, E.J.M. Hensen, Phys. Chem. Chem. Phys. 11 (2009) 2893–2902.

[31] E.A. Uslamin, B. Luna-Murillo, N. Kosinov, P.C.A. Bruijnincx, E.A. Pidko, B.M. Weckhuysen, E.J.M. Hensen, Chem. Eng. Sci. 198 (2019) 305–316.

[32] E. Kikuchi, M. Ogura, Catal. Surv. Jpn. 1 (1997) 227–237.

[33] A.A. Gabrienko, S.S. Arzumanov, A. V. Toktarev, D. Freude, J. Haase, A.G. Stepanov, J. Phys. Chem. C 115 (2011) 13877–13886.

[34] H. Himei, M. Yamadaya, M. Kubo, R. Vetrivel, E. Broclawik, A. Miyamoto, J. Phys. Chem. 99 (1995) 12461–12465.

[35] Z. Maeno, S. Yasumura, C. Liu, T. Toyao, K. Kon, A. Nakayama, J. Hasegawa, K. Shimizu, Phys. Chem. Chem. Phys. 21 (2019) 13415–13427.

[36] A.G. McKale, B.W. Veal, A.P. Paulikas, S.K. Chan, G.S. Knapp, J. Am. Chem. Soc. 101 (1979) 3763–3768.

[37] K. Nishi, K. Shimizu, M. Takamatsu, H. Yoshida, A. Satsuma, T. Tanaka, S. Yoshida, T. Hattori, J. Phys. Chem. B 102 (1998) 10190–10195.

[38] P. Honhenberg, W. Kohn, Phys. Rev. B 136 (1964) B864–B871.

[39] W. Kohn, L.J. Sham, Phys. Rev. A 140 (1965) A1133–A1138.

[40] G. Kresse, J. Furthmüller, Phys. Rev. B Condens. Matter Mater. Phys. 54 (1996) 11169–11186.

[41] G. Kresse, J. Furthmüller, Comput. Mater. Sci. 6 (1996) 15–50.

[42] P.E. Blöchl, Phys. Rev. B 50 (1994) 17953–17979.

[43] G. Kresse, D. Joubert, Phys. Rev. B 59 (1999) 1758–1775.

[44] J.P. Perdew, K. Burke, M. Ernzerhof, Phys. Rev. Lett. 77 (1996) 3865–3868.

[45] S. Grimme, J. Antony, S. Ehrlich, H. Krieg, J. Chem. Phys. 132 (2010) 154104.

[46] S. Grimme, S. Ehrlich, L. Goerigk, J. Comput. Chem. 32 (2011) 1456–1465.

[47] C. Baerlocher, L.B. McCusker, (2013). http://www.iza-structure.org/databases (accessed June 10, 2019).

[48] G. Li, E.A. Pidko, R.A. Van Santen, C. Li, E.J.M. Hensen, J. Phys. Chem. C 117 (2013) 413–426.

[49] M.W. Chase, C.A.D. Jr., J. J.R. Downey, D.J. Frurip, R.A. McDonald, A.N. Syverud, NIST-JANAF Thermochemical Tabels, 2nd ed., the U.S. Department of Commerce, Washington, DC, 1985.

[50] G. Henkelman, B.P. Uberuaga, H. Jónsson, J. Chem. Phys. 113 (2000) 9901–9904.

[51] W. Humphrey, A. Dalke, K. Schulten, J. Mol. Graph. 14 (1996) 33–38.

[52] K. Searles, G. Siddiqi, O. V. Safonova, C. Copéret, Chem. Sci. 8 (2017) 2661–2666.

[53] A. Getsoian, U. Das, J. Camacho-Bunquin, G. Zhang, J.R. Gallagher, B. Hu, S. Cheah, J.A. Schaidle, D.A. Ruddy, J.E. Hensley, T.R. Krause, L.A. Curtiss, J.T. Miller, A.S. Hock, Catal.

Sci. Technol. 6 (2016) 6339–6353.

[54] K. Reuter, M. Scheffler, Phys. Rev. B Condens. Matter Mater. Phys. 68 (2003) 045407.

[55] K. Reuter, M. Scheffler, Phys. Rev. Lett. 90 (2003) 046103.

[56] G. Li, P. Vassilev, M. Sanchez-Sanchez, J.A. Lercher, E.J.M. Hensen, E.A. Pidko, J. Catal. 338 (2016) 305–312.

[57] C. Liu, G. Li, E.J.M. Hensen, E.A. Pidko, ACS Catal. 5 (2015) 7024–7033.

[58] S. Li, Y. Wang, T. Wu, W.F. Schneider, ACS Catal. 8 (2018) 10119–10130.

[59] B. Ipek, M.J. Wulfers, H. Kim, F. Göltl, I. Hermans, J.P. Smith, K.S. Booksh, C.M. Brown, R.F. Lobo, ACS Catal. 7 (2017) 4291–4303.

[60] K. Mlekodaj, J. Dědeček, V. Pashkova, E. Tabor, P. Klein, M. Urbanova, R. Karcz, P. Sazama, S.R. Whittleton, H.M. Thomas, A. V. Fishchuk, S. Sklenak, J. Phys. Chem. C 123 (2019) 7968–7987.

[61] J. Dědeček, E. Tabor, S. Sklenak, ChemSusChem 12 (2019) 556–576.

[62] J.H. Lunsford, Catal. Today 63 (2000) 165–174.

[63] N.J. Gunsalus, A. Koppaka, S.H. Park, S.M. Bischof, B.G. Hashiguchi, R.A. Periana, Chem. Rev. 117 (2017) 8521–8573.

[64] L. Yuliati, H. Yoshida, Chem. Soc. Rev. 37 (2008) 1592–1602.

[65] M. Ravi, M. Ranocchiari, J.A. van Bokhoven, Angew. Chem. Int. Ed. 56 (2017) 16464–16483.

[66] K. Narsimhan, V.K. Michaelis, G. Mathies, W.R. Gunther, R.G. Griffin, Y. Román-Leshkov, J. Am. Chem. Soc. 137 (2015) 1825–1832.

[67] R. Palkovits, M. Antonietti, P. Kuhn, A. Thomas, F. Schüth, Angew. Chem. Int. Ed. 48 (2009) 6909–6912.

[68] E. V. Kondratenko, T. Peppel, D. Seeburg, V.A. Kondratenko, N. Kalevaru, A. Martin, S. Wohlrab, Catal. Sci. Technol. 7 (2017) 366–381.

[69] A.I. Olivos-Suarez, À. Szécsényi, E.J.M. Hensen, J. Ruiz-Martinez, E.A. Pidko, J. Gascon, ACS Catal. 6 (2016) 2965–2981.

[70] J.F. Hartwig, J. Am. Chem. Soc. 138 (2016) 2–24.

[71] R. Horn, R. Schlögl, Catal. Lett. 145 (2015) 23–39.

[72] Y. Hou, S. Nagamatsu, K. Asakura, A. Fukuoka, H. Kobayashi, Commun. Chem. 1 (2018) 41.

[73] T. Onishi, H. Abe, K.I. Maruya, K. Domen, J. Chem. Soc. Chem. Commun. (1986) 103–104.

[74] G.Y. Popova, T. V Andrushkevich, Y.A. Chesalov, E.S. Stoyanov, Kinet. Catal. 41 (2000) 885–891.

[75] Z.-J.J. Zhao, A. Kulkarni, L. Vilella, J.K. Nørskov, F. Studt, ACS Catal. 6 (2016) 3760–3766.

[76] M.H. Mahyuddin, K. Yoshizawa, Catal. Sci. Technol. 8 (2018) 5875–5885.

[77] A.A. Latimer, A.R. Kulkarni, H. Aljama, J.H. Montoya, J.S. Yoo, C. Tsai, F. Abild-Pedersen, F. Studt, J.K. Nørskov, Nat. Mater. 16 (2017) 225–229.

[78] V.I. Hart, M.B. Bryant, L.G. Butler, X. Wu, K.M. Dooley, Catal. Lett. 53 (1998) 111–118.

[79] E.A. Pidko, V.B. Kazansky, E.J.M. Hensen, R.A. van Santen, J. Catal. 240 (2006) 73–84.